Thermal Inertia as an Integrative Parameter for Building Performance

G.M. Soret[1*], P. Vacca[1], J. Tignard[1], J.P. Hidalgo[1], C. Maluk[1], M. Aitchison[2], J. L. Torero[1]

[1] School of Civil Engineering, Building 49 Advanced Engineering Building, Staff House Road, The University of Queensland, St Lucia QLD 4072 Australia.

[2]School of Architecture, Design and Planning, Wilkinson Building, The University of Sydney, NSW 2008 Australia.

Abstract

Traditionally, the energy efficiency properties of building envelope components are prescribed world-wide using the steady-state "U-value" where the insulation capabilities rely on the thermal conductivity of construction materials only. However, the heat flow through the building envelope is also restricted by the effect of other material properties combined in the form of the thermal inertia, a widely used parameter that can be controlled in the building environment through transient-state parameters such as the cyclic transmittance "u-value". By controlling the thermal inertia of the building envelope components key aspects of the building performance such as the building thermal, energy efficiency and fire performance can be evaluated in a holistic manner so that balanced design solutions are obtained without detriment affecting each other. Herein, it is proposed a holistic assessment method that uses a numerical model to obtain the thermal inertia of building components from their thermal insulating parameters to ultimately predict reaction-to-fire performance. The method includes a complementary thermal test to achieve reliable and realistic assessments that enable the analysis of aspects like the effect of construction imperfections. Two wall assemblies were built first to illustrate the method including the thermal test and finally to verify the method by conducting reaction-to-fire tests.

Keywords: Thermal inertia; Building thermal performance; Building fire performance; Cyclic transmittance; Material Flammability.

*Corresponding author: Tel.: +61 7 3365 3619; E-mail address: gerardo.soretcantero@uq.net.au

1 Introduction

From the heat transfer fundamentals applied to the semi-infinite solid, the thermal inertia is defined as the weighting factor that determines the temperature of the contact surface of two solids with different initial temperatures [1]. By doing this, the thermal inertia describes how sensible the materials are to temperature changes and hence to reach steady-state conditions (i.e. thermodynamic equilibrium). Therefore, the thermal inertia makes itself apparent only under thermal transient conditions. The Thermal inertia combines three intensive material properties: The thermal conductivity "k", the density "ρ" and the specific heat "c". It is therefore a physical quantity that can be measured. Generally, the thermal inertia is expressed as the square root of the product of these three properties "$\sqrt{k\rho c}$" with the units $\frac{J}{m^2 K\sqrt{s}}$ (SI) or simply as the product of the three, "kρc" with the units $\frac{W^2 s}{m^4 K^2}$ (SI) [2]. Materials with high thermal inertia require a significant amount of energy to change its thermal conditions.

In the building environment, the thermal inertia of materials is used in different building design disciplines. Regarding the building energy efficiency, given the international commitments to reduce emissions to fight global warming, the building design community is doing very important efforts to reduce the use of energy by improving the building thermal performance so that appropriate level of comfort for the building occupants is achieved. Traditionally, the insulating properties of construction materials has been characterised considering steady thermal conditions by using the U-value or its inverse the R-value where the thermal conductivity of materials is the key and unique material property. Prescriptive approaches that regulate acceptable values for a global thermal conductivity (R-Value, U-Value) are used to quantify energy-efficiency [3-5]. These global parameters rely on the steady-state description of heat transfer, and they can be obtained by means of standardised analytical procedures [6], standardised testing procedures [6], numerical models complemented either with the standardised Hot Box [7] or novel and simpler testing procedures validated against Hot Box measurements [8]. Numerous studies have explored both numerical methodologies and experimental methods highlighting advantages, a range of applicability and limitations [7-10]. This approach has been adopted traditionally, because it provides most of the information about the energy needed to maintain particular building indoor conditions [11]. However, this is a conservative approach, mostly geared towards to the design of heating systems in cold climates [12, 13]. Hence, even though heating is a transient process, it is traditionally approximated to a steady-state limit using the thermal transmittance U-Value. However, an effective path to optimise building thermal performance is by enhancing the evaluation of the insulating capabilities of construction materials by considering dynamic thermal conditions. The

most common characteristics insulating parameters used for this thermal approach is the cyclic transmittance "u-value" or the decrement factor "f" where the thermal inertia becomes the fundamental material property.

When it comes to control and to evaluate the building occupant's fire safety, the thermal inertia plays also a very important role since this is a key property to define reaction-to-fire characteristics of materials such as the onset of ignition and the ability of the material to spread fire. Recent fires involving building façades have raised questions about the effectiveness of current methods to assess the potential of these high energy efficient assemblies to sustain or enhance the impact of conventional fires [12]. The records show fires scenarios involving building components and assemblies which include high insulating and combustible materials since the 1990s (at least 30 in the UK alone) [14]. In the last fifteen years, there has been a dramatic increase in very visible building fires involving insulation materials all over the world, in the UK, China and the Gulf region. Table 1 shows representative fire scenarios involving combustible facades in different countries since 1991.

Table 1 Fires involving combustible facades and sources of ignition.

Country	Building	Year
UK	Residential tower – Bolton Cube (Bolton)	2019
Australia	Residential tower – Neo200 (Melbourne)	2019
Malasya	Residential building – EPF (Selangor)	2018
UK	Residential tower - Grenfell (London)	2017
UAE	Residential tower – The Torch (Dubai)	2017
UAE	Residential tower - Ajman Towers	2016
UAE	Address DownTown Dubai Hotel	2015
Australia	Residential building - Lacrosse (Melbourne)	2014
France	Residential tower - Mermoz (Roubaix)	2012
UAE	Residential tower - Jumeirah Lake Tower (Dubai)	2012
China	Royal Wanxin building (Shenyang)	2011
China	High-rise apartment (Shanghai)	2010
Hungary	Residential building (Miskolc)	2009
USA	Monte Carlo Hotel and Casino (Las Vegas)	2008
Germany	Residential building (Berlin)	2005
UK	Residential tower - Garnock Court (Irvine)	1999
UK	Residential tower - Knowsley Heights (Huyton)	1991

Generally, buildings present natural vulnerabilities associated with fires that can commence internally or in external areas such as balconies. Once the fire spread externally, the magnitude of the damage increases in a very significant manner. However, no research has been performed to date towards the development of an assessment method of building envelope components to achieve balance between both thermal and fire performance.

The relevance of the thermal inertia as material property can be observed beyond the building environment in other fields such as the renewable energy industry where the thermal inertia is used to highlight advantages with respect to more traditional power plants [15]. Further, in geophysical sciences, the thermal inertia is considered as a parameter of primary importance in the Earth and extra-terrestrial remote sensing because it controls diurnal and seasonal surface temperature variations in Earth [16] and Titan [17], and can be effectively used to correlate specific geophysical properties evaluated to improve the efficiency of vehicles operating in other planet such Mars [18]. The thermal inertia is therefore a parameter that is shared by different and varied scientific fields and as such provides an opportunity to connect their theoretical principles.

Therefore, a holistic assessment approach can be established based on a widely used material property that effectively can lead, in the building environment, to the achievement of optimum and balance design solutions. However, this research found that while many scientific disciplines use the thermal inertia as a quantitative material property, except for building fire safety, this parameter is not currently used directly in building thermal performance environment where it is implicit in other parameters that describe thermal response instead, as it will be described here after.

This study presents an integrated assessment method for building facades using the thermal inertia as the connecting parameter to achieve adequate levels of building comfort, energy-efficiency and fire performance. The method can be applied at early stages of the design process where no physical system is available. A more realistic assessment can be achieved if assembly systems are available for testing. This way the outcome of the assessment can be verified and enhanced by evaluating the influence on performance of features like construction imperfections. In this sense, this study includes the analysis of two different building systems that assist also to illustrate the method.

The next section of this chapter presents key aspects of the theory behind both thermal and fire performance with regards the thermal inertia, first to understand the problem and then to support the method proposed. Then, the integrated method and the materials used are described. Two assembly systems are used to illustrate the process and finally to verify the method. The results are then discussed, and conclusions presented.

2 Key theoretical aspects

2.1 Building thermal/energy-efficiency

In the building environment, the thermal inertia of materials expressed in his square root value is also called heat penetration, thermal effusivity and specific admittance [19], different names for the same property that can lead to confusion. If the thermal environment is cyclic, then the thermal inertia is subject to the period of a thermal cycle and is called Admittance "a" [3] or Thermal storage Coefficient "THC" [20] that describes the ability of the material to both conduct and store heat with the period of the thermal cycle. Hence, if the period of the cycle is very long (i.e. quasi steady-state thermal conditions), the effect of the thermal inertia becomes negligible. In the literature, it can be also found the "thermal inertia index", defined as a non-dimensional index number that relates the steady-state U-value with the Admittance "a" for a cyclic period of a day, both with units $\frac{W}{m^2K}$ (SI) [19-21]. However, some authors relates the thermal inertia with the effective thermal capacity of building components [22] or simply the thermal capacity [23].

Indeed, in the building environment, the thermal inertia is identified by the research community as a "complex phenomenon" and defined using a qualitative description of the *effect* observed on buildings subject to transient thermal conditions [24]. Precisely, it is the effect of the thermal inertia on building thermal performance what is usually evaluated by means of quantitative insulating parameters and not the thermal inertia itself. Furthermore, the quantitative insulating parameters are manipulated in a way such that factors are created and used instead. The most common is the decrement factor "f", a non-dimensional parameter well accepted by the building design community that represents a key parameter to evaluate the thermal response of buildings subject to cyclic thermal conditions [24-26]. The decrement factor or amplitude decrement is often expressed by Eq. (1) where the outdoor temperature amplitude is compared with the indoor temperature amplitude highlighting the potential of improving both indoor thermal comfort and their reduction of the use of HVAC systems, hence improving the building energy efficiency [19, 27-31].

$$f = \frac{A_i}{A_e} = \frac{T_i^{max} - T_i^{min}}{T_e^{max} - T_e^{min}} \quad (1)$$

Indeed, a transient thermal approach would deliver more accurate assessments of building envelope components and depending on the geographical locations may be more appropriate than the steady-state. The heat transfer

process within a building assembly is described by the transient energy conservation equation shown in Eq. (2), where "τ_w" is the characteristic time of a building assembly to achieve steady heat flow conditions expressed by Eq. (3) and "τ_c" the period of a particular thermal cycle.

$$\frac{\partial^2 \bar{T}}{\partial \bar{x}^2} = \frac{\tau_w}{\tau_c} \frac{\partial \bar{T}}{\partial \bar{t}} \tag{2}$$

$$\tau_w = \frac{L^2 \rho c_p}{k} \tag{3}$$

When buildings are considered to be subject to large daily temperature variations with respect low seasonal fluctuations, τ_w is no longer negligible with respect to τ_c, and a thermal performance assessment deeming pure steady-state conditions are no longer precise [8, 32]. Under these conditions, the characteristic time of a building assembly to achieve steady heat flow conditions τ_w can equal or be higher than the period of the thermal cycle τ_c and hence the solution of the one-dimensional Fourier continuity Eq. (2) is transient. Depending on the thermal analysis being studied, it can be followed by different methods to solve this expression. To address the effect of daily temperature variations on the building thermal performance, the periodic solution of the Fourier continuity equation can be used and building envelope componets insulation properties derived. Even though a sinusoidal thermal approach still includes big approximations to real-life environmental conditions, its accuracy is enough for the building design process in the early design stages, and its simplicity allows a valuable estimation of building indoor temperatures.

To identify the thermal inertia from the decrement factor, its expression has to be noted in terms of insulating properties as per Eq. (5) [3] that combines the transient-state based cyclic transmittance u-value with the steady-state transmittance U-value generally expressed by Eq. (4). The u-value is defined as the characteristic insulating property of a building system that defines the ability of the material to conduct heat when subject to a cyclic in-out heat flow with a period $\tau_{c.}$, and is expressed by Eq. (6) for homogeneous slabs which take into account isothermal conditions for the unexposed surface. The response of the exposed surface of the building system is characterised by the surface admittance "**y**", describing the ability of the surface to absorb or lose heat from/to the environment. For homogeneous slabs, this is expressed by Eq. (7) considering the slab is isothermal in the unexposed surface. Both characteristic parameters depend on the admittance "a" that describes the ability of the

material to both conduct and store heat with the period of the thermal cycle (Eq. (8)), and the cyclic thickness "τ", a dimensionless parameter that represents the thickness of the building system depending on its volumetric heat capacity (Eq. (9)). The cyclic thickness includes material properties combined in the form of the thermal diffusivity and the characteristic admittance in the form of thermal inertia (i.e. kρc).

$$U - value = \frac{1}{\left(\frac{L}{k} + R_{si} + R_{se}\right)} \tag{4}$$

$$\mathrm{f} = \frac{\mathrm{u-value}\ (\tau_c = \mathrm{day})}{\mathrm{u-value}\ (\tau_c \to \infty)} = \frac{\mathrm{u-value}}{\mathrm{U-value}} \tag{5}$$

$$\mathbf{u}-\mathrm{value} = \frac{\boldsymbol{q}_{\mathrm{unexposed\ surface}}}{\boldsymbol{T}_{\mathrm{exposed\ surface}}} = a\sqrt{\frac{2}{cosh(2\tau) - cos\ (2\tau)}}\, e^{\left(j\left(\frac{\pi}{4} - arctan\left(\frac{tan\ (\tau)}{tanh\ (\tau)}\right)\right)\right)} \tag{6}$$

$$\mathbf{y}-\mathrm{value} = \frac{\boldsymbol{q}_{exposed\ surface}}{\boldsymbol{T}_{exposed\ surface}} = a\sqrt{\frac{cosh(2\tau)+cos\ (2\tau)}{cosh(2\tau)-cos\ (2\tau)}}\, e^{\left(j\left(\frac{\pi}{4} - arctan\left(\frac{sin\ (2\tau)}{sinh\ (2\tau)}\right)\right)\right)} \tag{7}$$

$$a = \sqrt{\frac{2\pi}{\tau_c}\mathrm{k\rho c}} \tag{8}$$

$$\tau = L\sqrt{\frac{\pi}{\tau_c}\frac{\rho c}{k}} \tag{9}$$

The analytical procedure to obtain the characteristic parameters that describe the dynamic thermal response of building assemblies is described in detail in the literature [3, 11, 13, 19] and also standardised [33-35].

2.2 Building fire safety

Materials flammability is generally described by characterising ignition, heat release rate and flame spread. An enhanced heat release rate will increase the flame length and consequently accelerate the rate of spread. Heat release rate is, therefore, an important parameter when quantifying flame spread rates. Nevertheless, if the flame

is already spreading, the risk is already very significant. Therefore, it is more important to focus on the onset of the hazard; ignition is therefore the focus of this study.

A common way of characterising ignition is by means of the time to ignition, t_{ig}. The faster the time to ignition the more hazardous the material. Conveniently, another way of describing flame spread is as a series of ignitions across a solid surface, driven by the heat supplied by the flame. Therefore, a shorter time to ignition (also referred to as ignition delay time) results in a faster flame spread. Consequently, assessing time to ignition will indirectly characterise flame spread.

Modelling ignition and flame spread is very complex [36]. Nevertheless, many simplified approaches have been developed in the past. A commonly used expression to establish the time to attain an ignition temperature "t_{ig}" is the semi-infinite solid solution, simplified by Eq. (10). The sequence of ignitions leading to flame spread is described by means of an energy balance at the material surface as described by Eq. (11) [2], where "T_{cr}" is the critical temperature for ignition. This analysis is based on the inert heating of a material, and it was used by Hidalgo et al. to establish the failure criterion [37]. "T_{cr}" could thus be any critical temperature considered as a failure mode such as the temperature for ignition "T_{ig}" or the pyrolysis temperature "T_p", "T_{amb}" is the ambient temperature, $\dot{q}_e^{"}$ the heat flux received from a particular fire and "ϕ" the energy supplied by the flame to preheat the material [36]. Thermal conductivity, density and specific heat appear combined in the form of the thermal inertia "kρc".

$$t_{ig} = \frac{\pi}{4} k\rho c \left(\frac{T_{cr} - T_{amb}}{\dot{q}_e^{"}} \right)^2 \tag{10}$$

$$V_s = \frac{\phi}{k\rho c (T_{cr} - T_{amb})^2} \tag{11}$$

2.3 The thermal inertia as the connexion to overlap building component thermal and fire performance assessments

When the insulating capability of a building envelope component is optimised considering only the traditional steady-state U-value, then the targeted materials to be considered are those with the lowest thermal conductivity. By comparing Eq. (4) with Eq. (10) and Eq. (11), it can be clearly seen that the lower the thermal conductivity

value is, the lower the thermal inertia is and therefore, if the material is combustible, the lower the time that it takes to ignite is and higher rates of fire spread can be observed. Therefore, the problem is that materials that could be beneficial for thermal performance can become a fire hazard for building occupant's safety.

As described above, a transient analysis would deliver more accurate thermal performance predictions and might be necessary when the daily cycle is more representative of climatic conditions. When it comes to fire, being a rapid event, the thermal wave does not penetrate the integrity of the material. Therefore, the concept of the steady-state U-value only partially addresses the issues. Fire is a highly transient phenomenon where building material failure occurs much before a steady-state thermal condition is attained. Typical characteristic times for a fire event are of the order of 5-10 min to attain flashover [38]. All life safety measures need to respond within that period, so from the perspective of the safety of the occupants, the time to flashover represents well the fire time cycle. From Figure 1, it can be inferred that it is highly unlikely that a steady-state approach would be enough. Thus, when it comes to optimisation of both constraints, it is imperative to start the analysis using a transient thermal approach and hence material properties as the thermal inertia.

Generally, as the period of the thermal cycle τ_c increases, the cyclic transmittance u-value tends towards the steady-state transmittance U-value that represents the maximum capacity of building system for heat transmission. For building thermal performance analysis the period of the thermal cycle τ_c which is of interest, is the period of a day. The higher the thermal inertia the lower the u-value achieved with respect the U-value, therefore lower values of the decrement factor f. This implies lower heat gains (i.e. better thermal performance) in buildings located in geographical zones were daily temperature variations are representative and are also close to internal comfort temperature conditions. This approach is illustrated in Figure 1, where it can be seen how the capacity for heat transmission gets higher when the thermal period increases. In the figure, it is plotted the evolution of the u-value with increasing thermal periods of two building systems with the same U-value but different weight (i.e. different thermal inertia) together with the fire time cycle represented as the time to flashover. Both building systems have different insulating capabilities for a period of a day (i.e. first grey vertical colour line). Further information can be found in previous studies by Soret et al. [32] where the dimensionless decrement factor was used to analyse building thermal performance in Australia.

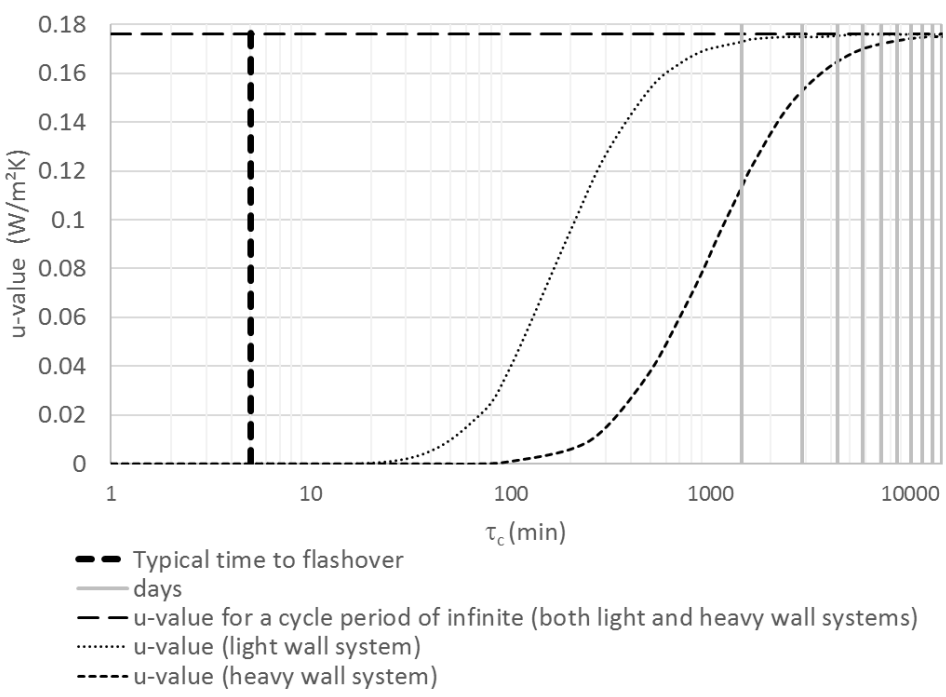

Figure 1 Variation of u-value with increasing cyclic periods with respect a typical time to flashover for a medium growth rate fire scenario.

From Eq. (6) and Eq. (8) it can be seen that the cyclic u-value thermal-efficiency parameter strongly depends on the thermal inertia (i.e. kρc) which also influence significantly flammability properties such as the ignition delay time described by Eq. (10) and flame spread velocity by Eq. (11). Hence, by characterising thermal-efficiency properties of building assemblies under cyclic transient conditions (i.e. u-value and y-value) the associated thermal inertia can be used to predict fire performance, thus enabling the development of the integrated assessment method for building components.

2.4 Measurement of dynamic insulating properties - thermal inertia.

The thermal inertia as well as the insulating properties of building envelope assemblies can be significantly influenced by other construction features such as structural elements and construction imperfections. To achieve realistic and detailed measurements of the thermal inertia of building envelope assemblies, this study searched first for available tests to measure this property. Alternatively, a test approach is developed to measure the thermal inertia of any building assembly.

Currently, there is no standardised procedure for measuring the characteristic insulating properties of building assemblies under transient cyclic thermal conditions [39, 40], therefore there is no standardized procedure to

measure the thermal inertia of building components. Nevertheless, some experimental procedures have been developed by adapting the standardised Hot Box experimental device [6] to measure insulating capabilities but not the thermal inertia itself. Brown and Stephenson developed experimental procedures adapting the standardised Hot Box facility so that programmed constant, ramp or sinusoidal temperatures could be applied on building assemblies [39]. It was demonstrated that the Guarded Hot Box could be used to define the frequency response of full-scale wall building assemblies and so they did for seven wall different building assemblies [41]. More recent studies have followed similar testing approaches to analyse the influence of structural elements acting as thermal bridges including transient effects [40, 42] where measurements were performed only at both external sides of a building assembly as represented in Figure 2. Given that the Hot Box was never intended to measure dynamic insulating properties and that no measured data is obtained from the interior of the system, the experiment approach, while useful, is inevitably limited.

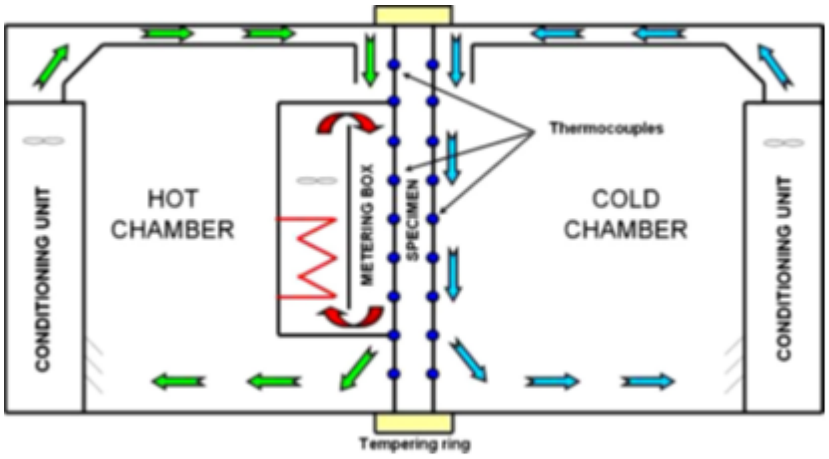

Figure 2 Representation of a Guarded Hot Box facility for testing in dynamic thermal conditions. Extracted from [40].

Also, there have been studies that measured the decrement factor experimentally according to Eq. (1) using the full experimental scale test room MINIBAT where a building assembly is placed between a climatic chamber and a solar simulator [43]. Another experimental apparatus used by the research community is the PASLINK test cell that follows an evolved testing approach from the European Passive Solar Components and Systems Testing (PASSYS) Project [44]. The testing approach is illustrated in Figure 3.

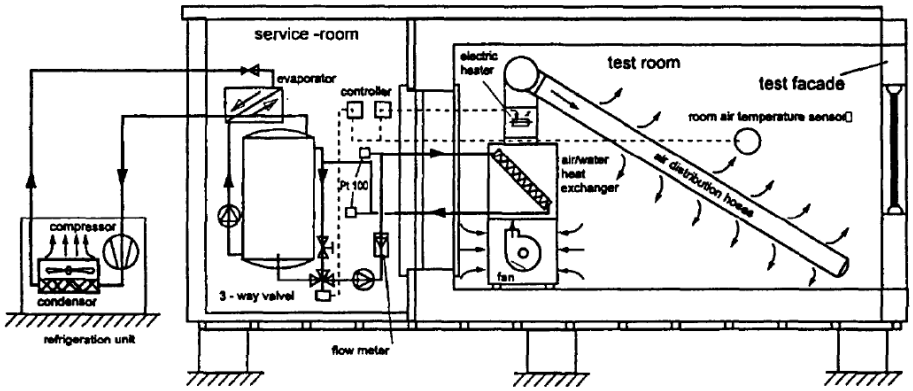

Figure 3 Representation of a conventional PASSYS-PASLINK test cell. Figure extracted from [45]

The research community have used the PASSYS test cell pursuing different objectives such as characterizing building envelope components performance under variable conditions [46, 47] and to validate simulation programs [44, 48]. The PASLINK testing approach and the classification of this test facilities are similar to that of the Hot Box facilities including additional limitations. It is acknowledge that this test presents a large and complex experimental approach, potential of high infiltration rates, limitation of the sample dimensions, high cost of the design and construction, longer testing periods than the Hot Box, detrimental influence of the maintenance of the facility to the measurements obtained among other issues that introduce a significant amount of unknowns and uncertainties, as well as those introduced by the thermal inertia and the thermal bridges of the cell itself [49].. There are internal test room air temperature measurements, internal test room surface temperature measurements, outdoors temperature measurements, solar radiation measurements together with other meteorological variables and heat flow measurements through the sample by using costly Heat Flux Sensitive Tiles (HFS Tiles) [47]. Nevertheless, only measurements from the exterior of the sample tested are obtained. No measurements are obtained for the interior so that the internal heat flow process could be used, for instance, to validate numerical models.

Along with the limitations described, all existing testing approaches rely on the variation of the temperature of the airflow, therefore, changing the heating condition is hugely cumbersome [10, 50-52]. Also, the heat flow through the assembly is a function of its thermal properties, and hence is very difficult to control. As a result, the error between measured and calculated transient response characteristics of a building assembly can be significant, especially when thermal inertia is high [10, 51]. Similar conclusions can be found in the literature regarding the standardised fire testing furnace [53, 54].

Given the limitations on the existing thermal testing approaches observed above, this study resolved to develop an affordable thermal test for building assemblies that enables:

- Internal measurements to obtain data including three-dimensional effects generated by structural elements and building construction imperfections
- The control of the heating boundary condition so that this could be varied in a systematic way for statistical analysis.

The thermal test can be used then to populate a numerical model to perform fully validated calculations. By doing this, the integrated method proposed hereafter is provided with realistic and detailed information of the thermal inertia of building envelope components.

3 Materials and methods

The integrated assessment method proposed in this study consists in predicting the ignition delay time of any building assembly with combustible materials using the thermal inertia measured from dynamic insulating properties. It can be applied at early stage of the design process where no physical system is built yet. However as introduced, a more detailed and realistic assessment can be achieved if assembly systems are available for testing to evaluate relevant aspects that may affect strongly performance like construction imperfections.

The proposed integrated assessment method is composed of four main steps. First, a numerical model that solves the transient energy equation for the building system is developed. Generally, if physical building assemblies are available, a small-scale thermal testing “SSTT” defined in this study can be conducted. The dimensions of the building system sampled are not constrained by the testing procedure. The experimental approach allows the definition of all testing conditions in a systematic way to obtain the necessary parameters (i.e. material properties) to achieve a numerical model that provides a realistic representation of the system following an inverse method [8].

Once a numerical model is achieved, it is used together with a spreadsheet for the calculation of the magnitude of both the u-value and the y-value at different points of the side of the building system under assessment. Considering sufficient points evenly distributed over the multilayered system, the overall u-value and y-value can be obtained. This approach can also be used to calculate the overall U-value of the multilayered system.

Then, both the u-value and the y-value calculated are assumed to be the characteristic insulating parameters of a hypothetical monolayer system. Under this approach and by using a non-linear systems of equations using respective analytical expressions, the cyclic thickness τ and the characteristic admittance "a" can be obtained, and from the later, the pursued thermal inertia.

Finally, the thermal inertia obtained is used to predict fire performance. The steps of the integrated method are described in detail in the following points together with the materials used.

3.1 FEM calibration from SSTT

If physical building systems are available, then thermal tests can be conducted to achieve detailed and realistic results. The thermal test defined is simple and affordable, so that the testing procedure can be readily followed by which a building system is monitored *both* internally and externally so that temperatures can be tracked spatially and temporally. The materials used are detailed in previous studies [8]. Different heat flux loads can be achieved at the exposed surface of a building system by varying the distance to the radiant heater. Heat flux values are defined by locating a heat flux meter in-lieu the system to measure the incident heat flux at different distances before testing.

Because the heat flow process is characteristic of the building system, the parameters driving heat transfer are the same independent the heat flux load. Then, building systems are exposed to the radiant heater at three different heating rates in a systematic way from ambient temperature until steady heat flow conditions within the system are attained. An electric radiant heat source is used to apply heat flux loads on the surface of the building system within the ranges of early stages of typical pre-flashover fires in a way such there is no material degradation.

In all cases, the building systems are monitored both internally and externally using thermocouples located at different depths of the system. Recorded measurements are compared with the numerical model representing the test approach. Following an inverse method, the best fit to the necessary numerical parameters can be obtained. One heat flux is used for numerical fitting purposes and the other two for validation.

It is important to note that transient temperature profiles of the system layers are interrelated. Thus, altering the thermal properties of the material of one layer affects the transient performance of the whole assembly [55]. For

this reason, only the material that occupies the largest volume in the system is used in this study to obtain the numerical fitting parameters. All the other materials and their associated properties are less representative in the volume of the system and thus their impact on the overall performance lower. Accordingly, these material properties are obtained independently from Hot Disk Thermal Constant Analyser measurements where the transient plane source technique (TPS) is followed, whose details can be found in the literature described by the research community dealing with construction materials [56]. Hence, these properties were assumed valid for the model. As a result, a model is obtained representing realistic internal heat flow processes that allows the evaluation of construction details such as material imperfections or contact resistances. The systematic variation of the heating load allows obtaining enough data to deliver statistically valid data assimilation.

3.2 Transient cyclic thermal parameters calculation

While there are specific tools developed to quantify both u-value and y-value of building assemblies [57], this study uses the more general approach of using a Finite Element Model (FEM). For this study the thermal transient module of ANSYS® Workbench V15 was used. The boundary conditions considered for the numerical model along with the heat load condition following a sinusoidal pattern. This is represented in Figure 4a and Figure 4b for a single monolayer building system where a sinusoidal heat flux load is applied at one surface denoted "1", deeming isothermal conditions at the unexposed surface denoted "2" (i.e. $T_2 = 0$). Generally, the amplitude of the net heat flow wave "$\dot{q}''_{net}(t)$" decays exponentially as it passes through the material (Figure 4a). An insulation layer with low mass would make the amplitude of the temperature be reduced significantly at the unexposed surface because of its low thermal conductivity. However, the amplitude of the heat flow at the unexposed surface would be similar to that of the exposed surface yet slightly lower. In the limit, if no mass is considered, the amplitude of both surfaces is the same as illustrated in Figure 4b.

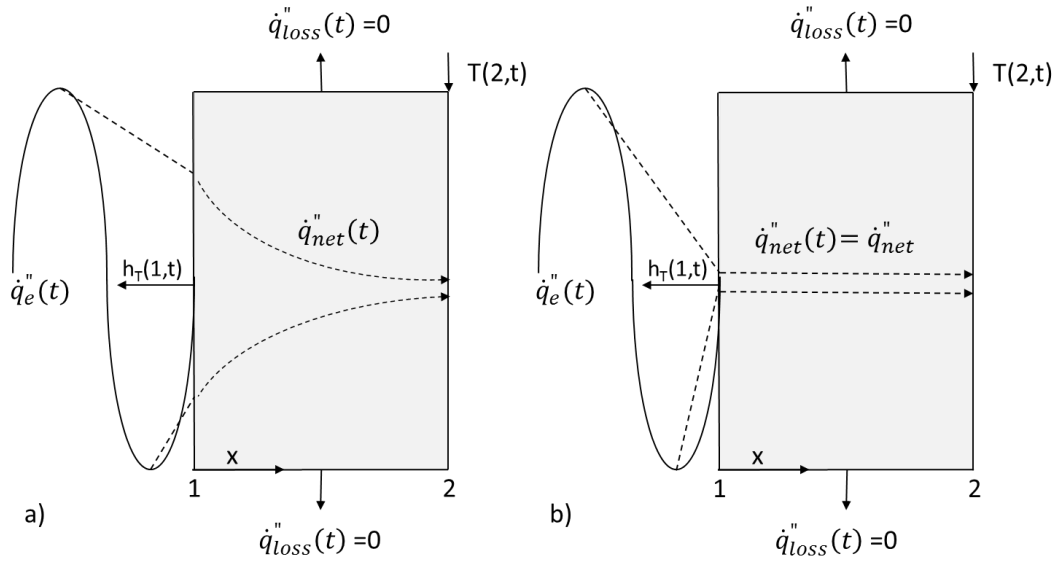

Figure 4 Thermal conditions for the definition of: a) u-value b) U-value (no mass)

Edge boundary conditions in the model are assumed to be adiabatic over time, and an initial condition is included as represented in Eq. (10). Eq. (11), which represent the sinusoidal heat load applied to the exposed surface with amplitude "A" and a cyclic period τ_c of a day. A total heat loss coefficient h_T is assumed not to be time-dependent and is applied to this surface according to Eq. (12). The unexposed surface includes an isothermal condition as expressed by Eq. (13).

$$T(x,0) = T_2 = T_{amb} \tag{10}$$

$$\dot{q}''_e(t) = A + Asin\left(\frac{2\pi}{\tau_c}t\right) \tag{11}$$

$$\dot{q}''_{net}(t) = -k\frac{\partial T}{\partial x}\Big|_1 = \dot{q}''_e(t) - h_T(T_1 - T_{amb}) \tag{12}$$

$$\mathrm{T}(2,\mathrm{t}) = T_2 \tag{13}$$

While the heat transfer within the assembly is three-dimensional because of the effect of structural elements, the overall heat transfer remains one-dimensional. The FEM outputs are both the exposed and unexposed surface sinusoidal temperature histories and the heat flow-time histories at a point of the system. From this data with the aid of a spreadsheet, wave amplitudes can be quantified to finally calculate the magnitude of both u-values and y-values at the point deemed in particular. When both parameters are obtained for a number of points disposed evenly in a matrix form at the exposed surface (white cross-dots in Figure 5), average u-values and y-values of the matrix data can be obtained that include the effect of structural elements.

To verify this approach, the overall u-value of the system is calculated when no volumetric heat capacity (i.e. no mass) is input in the model. Thus, the overall U-value of the system is calculated numerically under cyclic transient conditions including the effect of thermal bridges. Ultimately this is compared with the overall U-value obtained in previous studies under a steady-state thermal approach [8]. This way, the deviation obtained gives calculation accuracy so that the density of points included in the form of a matrix can be increased if deemed appropriate.

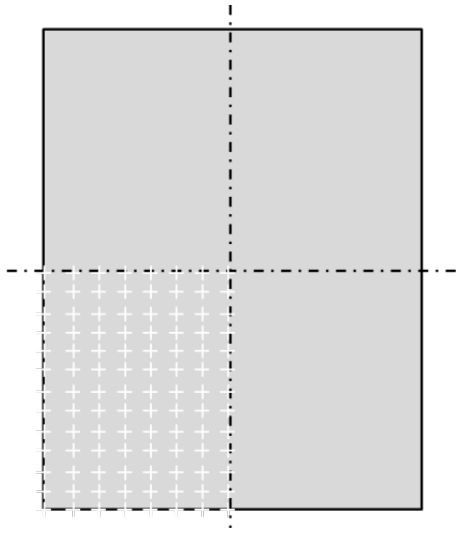

Figure 5 Front view of a hypothetical building assembly sampled and a representation of a possible arrangement of matrix data (white marks)

3.3 Extraction of the energy-efficiency based thermal inertia.

Once the magnitude of both the u-value and the y-value at the surface of a multilayered building assembly are obtained, they are considered as the characteristic insulating parameters of a representative homogeneous system. Hence, Eq. (6) and Eq. (7) can be used and a non-linear system can be established and easily solved by using MATLAB® to obtain both the characteristic admittance "a" and cyclic thickness "τ". Finally, from the characteristic admittance expression (Eq. (8)) it can be obtained the thermal inertia at the exposed surface (i.e. kρc) of the multilayered system.

3.4 Integrated assessment with fire safety

If ignition delay time is to be estimated, the value of the thermal inertia at the exposed surface is enough as per Eq. (10). The critical temperature for ignition of the material exposed can be estimated from existing data in the

literature, using standardised tests [58] or by following the procedures described by Hidalgo et al. [37], and the incident heat flux, "$\dot{q}_e^{"}$" , from the fire scenario to be analysed.

In the following section, this method is illustrated by estimating the ignition delay time of two different building systems with plywood exposed.

4 Case studies

To illustrate the proposed method, two systems of each assembly approach were built containing all relevant construction elements following standard manufacturer and builder practices. More details about both systems assessed in this study can be found in previous studies [8]. Results are presented herein and used in the following section to verify the method proposed by conducting reaction-to-fire tests.

The first building assembly is a 1200 mm length by 900 mm width light steel frame "LSF" with a frame composed of C-shaped steel studs on the edges of the system along with a steel stud located in the middle of the shorter side of the panel. The voids created by the steel frame are filled with 92 mm of Glass wool insulating material. The external cladding is formed by 12 mm plywood panel and the internal lining is a 12mm plasterboard panel. An 18 mm air cavity is created by placing timber battens between the steel frame and the plywood panel.

The second case is a load-bearing structural insulated panel "lbSIP+Ply", whose overall dimensions were 800 mm of height and 600 mm of width. This multilayered system was geometrically symmetrical both vertically and horizontally and comprised of 144 mm thick expanded polystyrene foam (EPS) core enclosed by 12 mm MgO (Magnesium oxide) panels on the main surface and 30 mm MgO on the edges including a MgO spline mid-width as a load-bearing element. The external cladding was a 12 mm plywood panel, the same material as the LSF system to enable the assessment of flammability properties.

4.1 FEM fitting parameters.

In this study, the information analysed from the SSTT is the temperature history along the transient period when the system is exposed to different thermal heat loads achieved by placing a radiant heater at different distances from the system. The fitting material properties are obtained by following an inverse method using both the SSTT data acquired and the numerical model representing the testing approach. Only the most representative material

occupying the largest volume in the system was used in this study to obtain the numerical fitting parameters. The material properties of the other materials less representative were measured independently by using the TPS technique mentioned before.

Per the methodology, different heat flux loads at the system surfaces within the range of typical pre-flashover fires were defined and measured using a flux meter placed at different distances from the radiant heater. Table 2 presents these data together with the heat flux values applied to each system. Low softening temperature point was observed for the EPS core material in preliminary tests (i.e. below 100°C). In order to prevent EPS deterioration and avoid measurement deviations by the effect of air voids created in the EPS volume the series of SSTT were performed at lower heat flux values so that the interface MgO-EPS did not reach EPS softening points temperatures.

Table 2. Nominal heat fluxes measured at the exposed surface for numerical model fitting and for the validation of predicted values using obtained fitting parameters.

Distance from the heater (mm)	Max. heat flux measured at the system surface (kW/m²)	LSF	lbSIP+Ply
425	4	Validation	
680	1.92	Fitting	
825	1.34	Validation	Validation
925	1.11		Validation
1025	0.89		Fitting

Because during the tests the materials were not degraded, all parameters were considered constant values. In the model, thermal conductivities of the materials, surface emissivity coefficients and total heat transfer coefficients inputs were those obtained in previous studies [8]. Densities and specific heat of system materials were measured by a Hot Disk Thermal Constant Analyser, except for the air cavity, the steel frame and the reflective foil that were obtained from generic values found in the literature. From this starting point, the inverse method started, so that fitting properties (i.e. density and specific heat) of insulating materials were finally achieved.

To set the end-point of the inverse process, three calculated temperatures taken evenly along the whole heating period from the heater were compared with those measured at matching times. A mean deviation between calculated and measured temperature histories lower than 8 % was assumed to be good enough. Figure 6 shows the temperature history of both measured and calculated for the insulating materials of the systems at three points located at different depths from the unexposed surfaces. Error bars indicate the standard error from mean temperatures measured where the maximum value observed for all the test was 8.4 °C.

Finally, numerical fitting data was obtained so that a realistic assessment could be achieved. Table 3 and Table 4 include the results for both the LSF and the lbSIP+Ply systems.

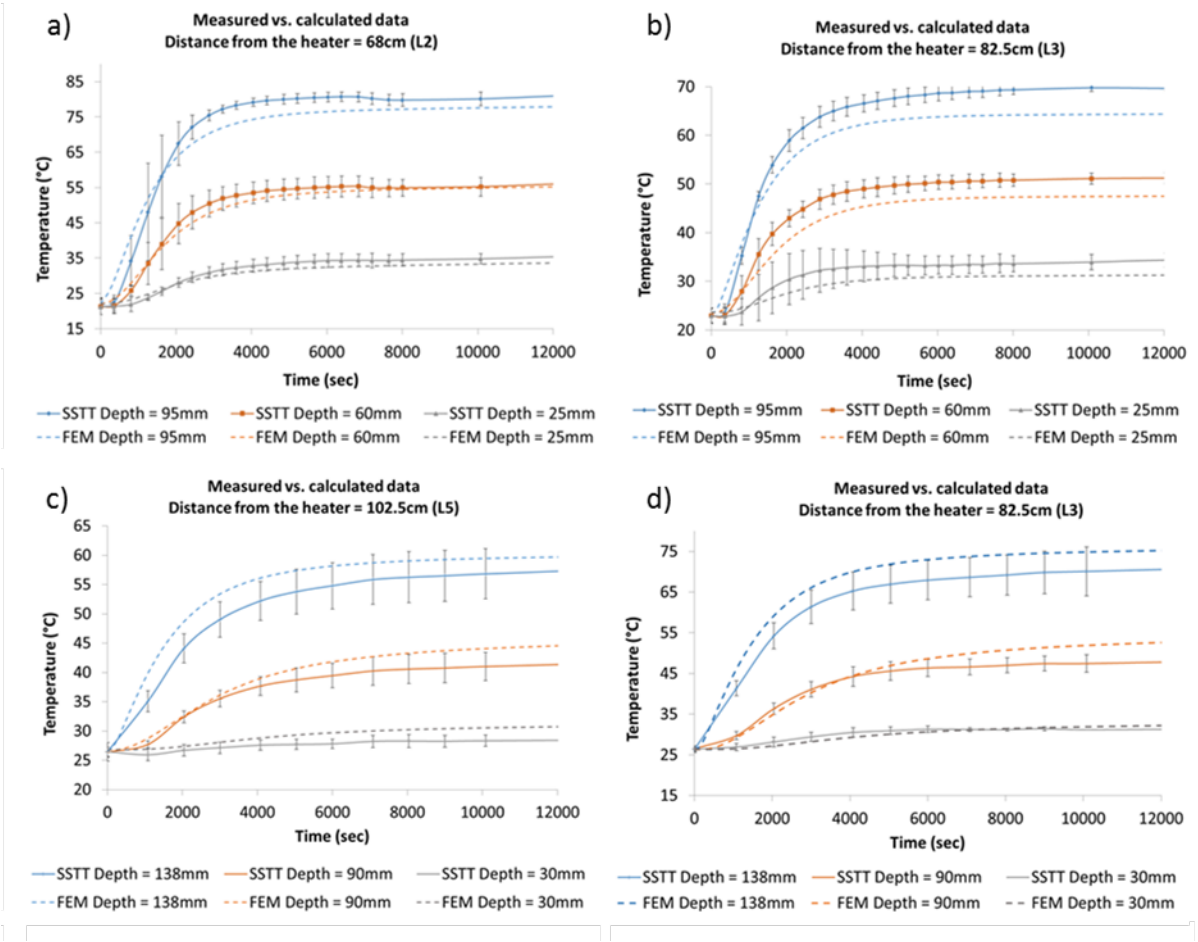

Figure 6 Measured and calculated temperature-time history in both the LSF and lbSIP+Ply systems – insulating material: a) and c) Tests to extract fitting parameters - LSF and lbSIP+Ply systems respectively. b) and d) Tests to validate predicted values using fitting parameters - LSF and lbSIP+Ply systems, respectively.

Table 3 FEM fitting material properties input values for the LSF system case. (*) Measured in previous studies [8]. (**) Properties measured independently by using Hot Disk Thermal Constant. (***) Properties from literature.

Material	Thermal conductivity (W/mK)	Density (kg/m^3)	Specific Heat (J/kgK)
Plywood	0.183*	492**	1375**
Timber Batten	0.173*	613**	903**
Reflective Foil	2.000*	400***	500***
Steel Frame	30.000*	7833***	465***
Mineral Wool	0.033*	15	1248
Plasterboard - Internal Lining	0.234*	658**	1092**
Air cavity	0.017*	1***	1005***

Table 4 FEM fitting material properties input values for the lbSIP+Ply system case. (*) Measured in previous studies [8]. (**) Properties measured independently by using Hot Disk Thermal Constant.

Material	Thermal conductivity (W/mK)	Density (kg/m^3)	Specific Heat (J/kgK)
Plywood	0.183*	492**	1375**
MgO	0.357*	830**	1550**
EPS	0.026*	16	1756

4.2 Characteristic energy efficiency parameters under cyclic transient conditions

Once a realistic numerical model of a system is achieved, it can be used to calculate the magnitude of both u-value, y-value together with the steady-state U-value by considering the mass negligible. Average values can be obtained from local values at different points of the system that can be distributed evenly in matrix form to account for all inhomogeneity of the system (i.e. structural elements). This approach can be verified by comparing the average U-value calculated with other experimental methods conducted in steady thermal conditions [6, 8].

To represent this approach, the matrix data obtained for the lbSIP+Ply panel is represented in Figure 7a and Figure 7b. It included 1,271 points in total where all U-value, u-value and y-value were calculated. The deviation obtained was lower than 5% when compared to the average U-value of all points calculated, with previous estimations of U-value from different steady-state tests with the same system [8]. In this study, such deviation was assumed acceptable to calculate average values for both u-value and y-value for ulterior integrated fire performance estimation and hence the density of the matrix data enough. Nevertheless, if more accuracy was needed, a denser matrix could be considered.

Figure 7a and Figure 7b shows that both u-values and y-values have higher values in those areas closer to the internal structural elements acting as thermal bridges because their higher capacity to conduct, absorb, store and release heat to the environment.

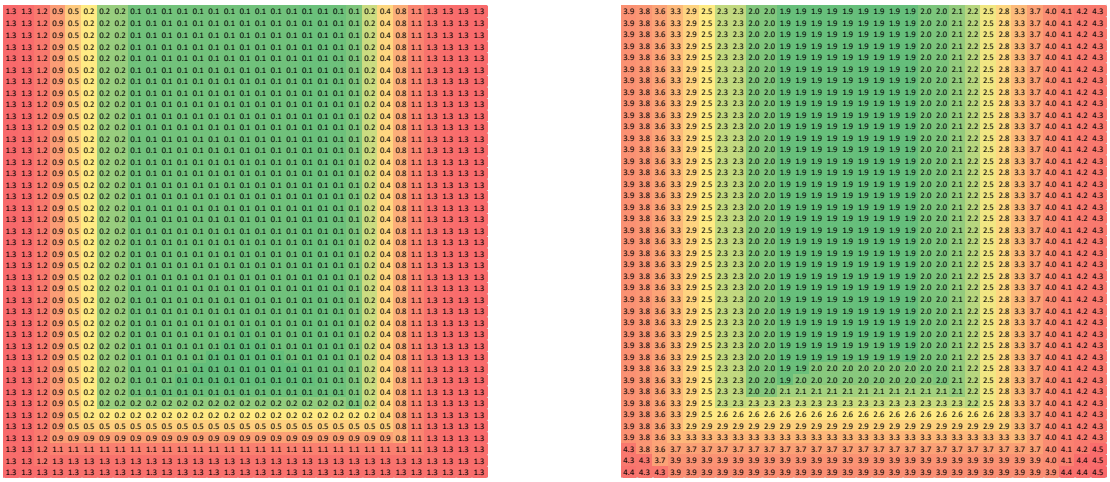

a) b)

Figure 7 Calculated u-value (a) and y-value (b) at points in matrix distribution for the left-bottom area of the lbSIP+Ply system (Units in W/m^{2}K).

Table 5 shows the overall u-value of both the LSF and the lbSIP+Ply systems and the y-value of the exposed surfaces together with the analytical values calculated for the ideal homogeneous multilayered systems. The thermal bridge effect by the internal load bearing MgO spline is significant since the ability to conduct heat through the system under cyclic conditions is increased by 229%. In the case of the LSF system, this is increased by 181%. Similarly, the ability to absorb and release heat is increased by 56% in the lbSIP+Ply system and by 68% for the LSF system by structural elements indicating that these structural elements contribute to achieving a more stable building indoor temperature.

Table 5 Comparison of overall thermal efficiency magnitudes under cyclic transient conditions.

Building assembly	Overall u-value magnitude (W/m^{2}K)	Overall y-value magnitude (W/m^{2}K)
lbSIP+Ply system	0.56	2.77
Ideal homogeneous lbSIP+Ply system	0.17	1.78
LSF system	0.7	1.09
Ideal homogeneous LSF system	0.25	0.65

4.3 Calculation of the energy efficiency based thermal inertia.

Once the energy efficiency parameters are calculated local values distributed in matrix form of the apparent thermal inertia at the exposed surface of the system can be obtained and represented. This is illustrated in Figure

8 for the lbSIP+Ply system. In this case, the maximum apparent thermal inertia of 295,836 W^2s/m^4K^2 is achieved at those points which directly correspond to the physical location of the structural elements. The apparent thermal inertia reduces gradually to a minimum of 47,875 W^2s/m^4K^2 until influenced by another structural element. Adiabatic boundary conditions are presented at edges where no heat losses are presented (and hence the apparent thermal inertia would be zero).

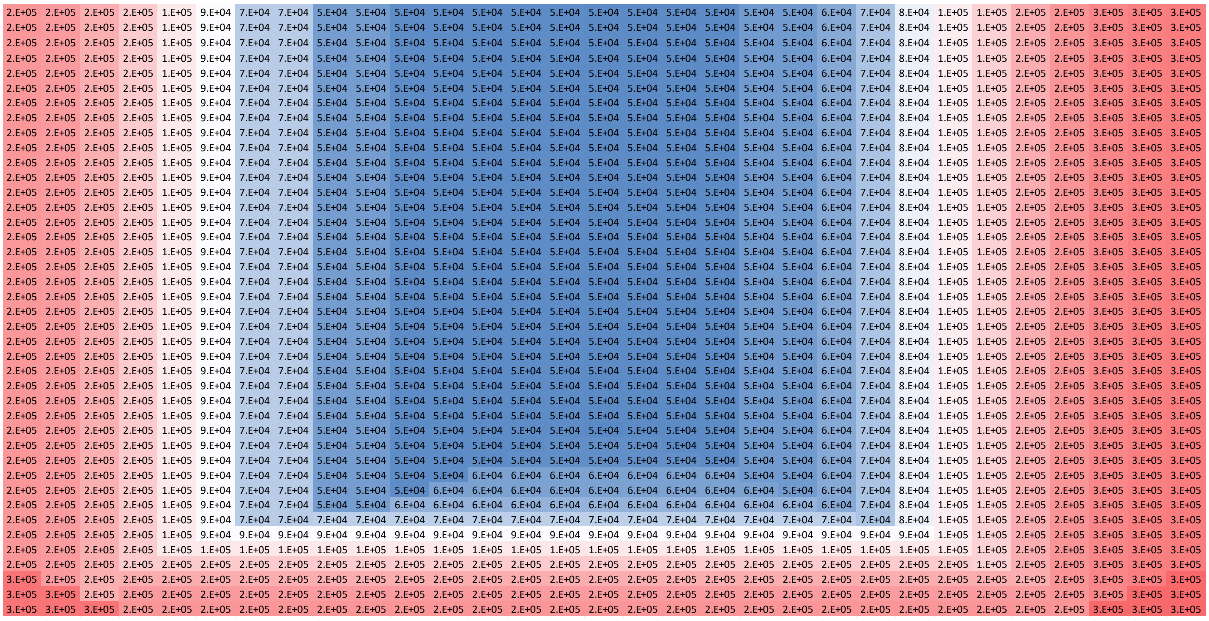

Figure 8 Calculated thermal inertia (W^2s/m^4K^2) at points distributed in matrix form for the left-bottom area of the lbSIP+Ply system

4.4 Integrated assessment: Estimation of time delay to ignition.

By taking an average value of the thermal inertia including all points included in the matrix distribution considered, this study treats the attainment of the critical temperature as an average value that takes into account the complexity of the whole building system. For the lbSIP+Ply system according to Figure 8 data, this value results in 124,801 W^2s/m^4K^2. For the LSF system, this value results in 18,355 W^2s/m^4K^2. Table 6 includes estimated overall time delay to ignition values for different incident heat fluxes $\dot{q}_e''$. There was no system available to evaluate piloted ignition in a systematic way at the time this study was performed so it was decided to focus on critical temperatures for autoignition, which for plywood was assumed 600°C in line with data obtained in the literature for wood [20]. According to other studies, this would represent a conservative value since ignition surface temperatures for incident heat fluxes below 40 kW/m^2 reached a constant value of 700°C or higher [59].

Table 6 Time delay ignition estimated for different incident heat flux values

	t_{ig} (seconds)	
$\dot{q}_e^{"}$ (kW/m^2)	lbSIP+Ply	LSF
35	27	4
30	37	5
25	53	8
20	82	12

5 Verification of the method

In order to evaluate the results obtained, herein it is compared the calculated ignition delay time with measured data from reaction-to-fire -tests applied to both the LSF and the lbSIP+Ply systems. The estimated values are assumed to be unavoidably conservative because fire is a much rapid event than the cyclic thermal model from where insulating properties are defined. Herein it is presented a reaction-to-fire fire test performed.

5.1 The radiant panel test set-up

The radiant panel test defined in this study is simple and affordable, so that the testing procedure can be readily followed and by which a building system is monitored internally and externally. A heat source is used to apply a heat load on one surface of the building system from ambient temperature until steady heat flow conditions within the system are observed. This study uses two GoGas Radimax porous burners radiant panels put together to achieve a rectangular shape of 0.4 m length and 0.15 m height and that were mounted to a metal frame as shown in Figure 9a and Figure 9b. These are lightweight radiant panels and provide rapid thermal responses during both the heating and cooling periods, together with high and stable operational temperatures and thermal homogeneity at the emitting surface. The type of gas used was Natural gas. A movable air blower, an air train and a gas train unit are connected to a control panel. They supply air and natural gas flow to the radiant burner panels by specific hoses and controls burners ignition.

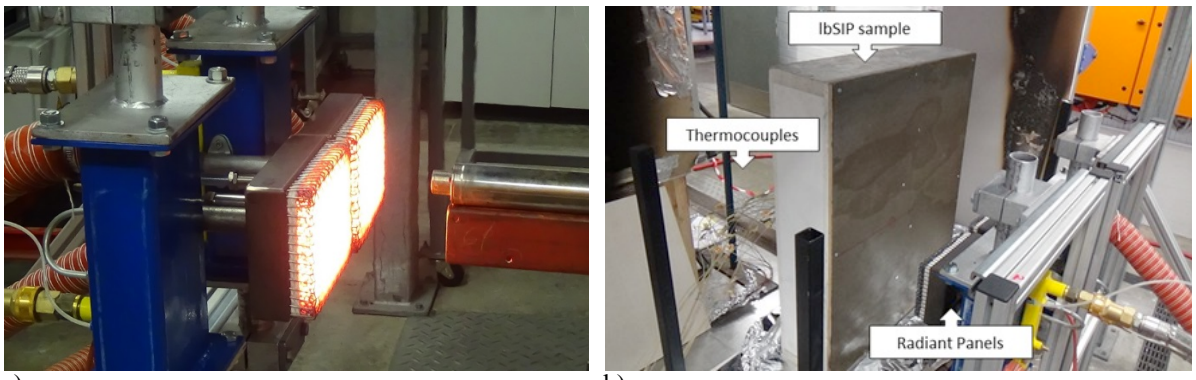

a) b)

Figure 9 Small scale radiant panel experimental set-up for the lbSIP+Ply wall system

Ambient temperature was measured and recorded during tests by an RTD thermocouple together with temperature histories that were measured and recorded across each layer of a system by thermocouples located at different depths. For this, type "K" thermocouples were used for both building systems (i.e. LSF and lbSIP+Ply). Thermocouples were inserted from the unexposed surface to avoid possible deviations in temperature measurements caused by heating the thermocouples wire (Figure 9b). Recorded temperature data was used to analyse in-depth temperature histories of test samples.

To account for a more refined evaluation including the effect of structural elements on the system, temperature histories were measured in each layer in regions closer to and further from the structural elements. Thus, at least two aligned series of thermocouples were located in the building systems tested in the same way described in previous studies [8] for the LSF system case.

Finally, tests were recorded with a video camera placed in front of the building system so that ignition delay times were measured to be ultimately compared with estimated ignition delay times calculated by using the integrated assessment developed by this study.

5.2 Measurement of incident radiant heat fluxes

To measure the incident radiant heat flux $\dot{q}_e^{"}$ at the target exposed surface of the test sample, a pre-test calibration procedure was performed by using a heat flux meter (SBG01 Hukseflux) mounted on a self-cooling probe system designed to minimise the influence of convective flows near the gauge as showed in Figure 9a. It was used to quantify the heat flux provided by the radiant panels at distances. Then, by placing building assemblies with the

target surface placed at these distances a precise incident radiant heat flux $\dot{q}_e^{"}$ received by the surfaces was known for each distance.

For this method two distances from the radiant panels were considered, 210 mm and 180 mm, to study two different levels of thermal loads. A heat flux measurement at these distances was performed. Thus, the heat flux meter was placed at each distance, so that heat flux intensities were measured. For precision, the heat flux value at each distance was defined as the average value of 9 points measurements distributed evenly following a two-dimensional rectangular grid according to the radiant panel area as represented in Figure 10.

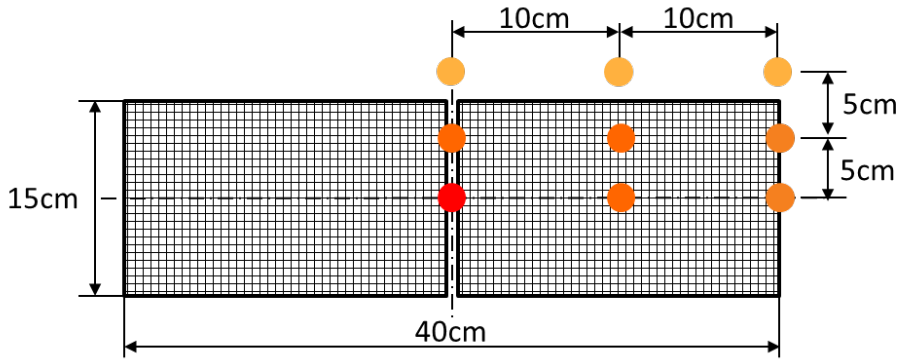

Figure 10 Front view representation of the radiant panels with the points where heat flux measurements where performed

As a result, a mean heat flux value of 24 kW/m^2 with a standard deviation of 0.2kW/m^2 was measured for 210 mm from the radiant panels, and 29 kW/m^2 with a standard deviation of 0.4kW/m^2 when the separation distance was 180 mm. To achieve the desired incident radiant heat flux at the exposed surface of the sample, during the initial heating phase of the radiant panels the sample was shielded with the aid of a plasterboard panel, which was placed between the sample and the radiant panels; until these were steady (less than 5 minutes). Thus, ignition delay time was measured from the moment that the shield was removed until sustained burning was observed.

5.3 Verification of critical temperature for ignition (T_{cr})

Temperature measurements at surfaces are difficult to achieve by using thermocouples because measurements are unavoidably influenced by convection processes at the surface magnified by the deterioration of the material surrounding thermocouple heads due to the high incident heat fluxes. Instead, it is decided to measure the surface temperature history of the plywood panel by using a FLIR SC 655 infrared camera. Only one measurement could be done in this study and it was during the radiant panel test for the lbSIP+Ply panel placed at 180 mm from the radiant panels (29 kW/m^2).

Figure 11b shows the temperature history measured of the exposed surface of plywood where it can be seen the increment of temperature from the moment the thermal shield placed between the radiant panels and the system was removed to the time were ignition with sustained flames were observed. Considering data measured contained in the box1 in Figure 11a at this time it was measured an average critical temperature for ignition T_{cr} of 553°C with a standard deviation of 238°C at ignition time. This value differs 8% from the critical temperature for ignition used on case studies to estimate t_{ig}. For simplicity and to also compare easily estimated ignition delay values in those points, the measured T_{cr} used to validate extracted apparent thermal inertia values was the value found in the literature (i.e. 600°C).

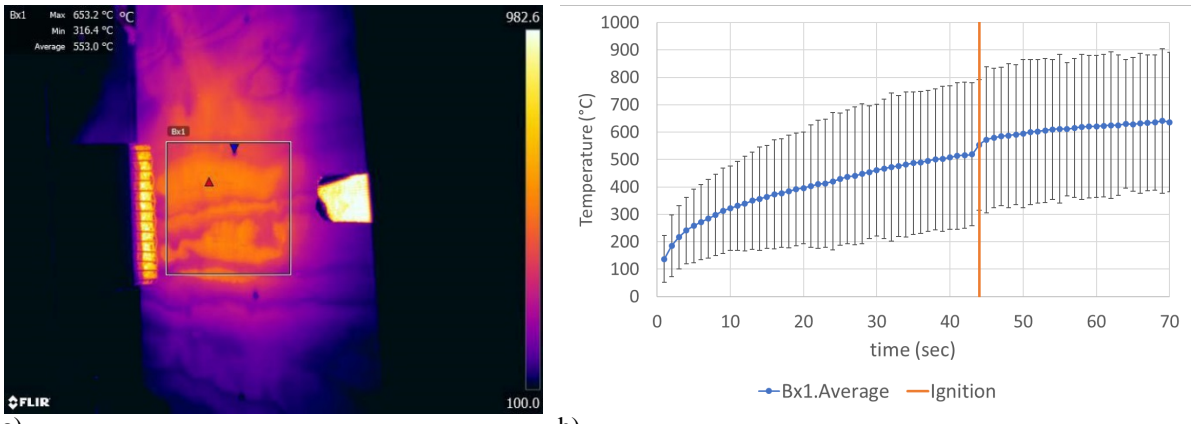

a) b)

Figure 11 lbSIP+Ply system with an incident radiant heat flux of 29kW/m²
a) Infrared camera frame at ignition time. b) Temperature history measurement at the exposed surface of the

5.4 Measured and calculated data

This methodology was applied to measure ignition delay times and internal temperature histories at different depths of four LSF system samples and four lbSIP+Ply systems for analysis, so that two tests were performed for each radiant heat flux. All radiant tests were conducted using the same tests set-up and data used to describe the method proposed.

As described previously, ignition delay times were calculated according to Eq. (10) using apparent thermal inertia values extracted from the thermal insulating properties, measured incident heat fluxes (24 kW/m^2 and 29 kW/m^2) and measured critical temperature to ignition T_{cr}. The latter, however, was assumed to be the value found in the literature (600°C) because it was closer to the unique measurement that could be performed in this study and for simplicity when comparing to estimated values outlined in previous sections.

The ambient temperature measured in the environment where the radiant panel tests were performed changed with time. As mentioned, for ignition calculation purposes this value is not relevant, so it was considered for all calculations to be 20°C. Table 7 includes measured ignition delay times from tests, and Table 8 compares ignition delay time calculated with mean values measured for each heat flux applied.

Table 7 Measured ignition delay times values: Two samples each system case tested per the incident radiation heat flux considered.

Sample	Mean Heat Flux (kW/m^2)	Ignition delay time measured (sec)
LbSIP+Ply – A1	24	No ignition
LbSIP+Ply – A2	24	No ignition
LbSIP+Ply - B1	29	44
LbSIP+Ply – B2	29	39
LSF - A1	24	505
LSF - A2	24	595
LSF - B1	29	48
LSF – B2	29	38

Table 8 Calculated and measured ignition delay times values

Sample	Mean Heat Flux (kW/m^2)	Mean Ignition delay time measured (sec)	Ignition delay time calculated (sec)
LbSIP+Ply	24	No ignition	59
LSF	24	550	9
LbSIP+Ply	29	42	40
LSF	29	43	6

Figure 12 includes temperature histories of the systems recorded at different depths. Recorded temperatures started when the protecting panel placed in front of the sample was removed. Tests finished when steady temperature conditions were observed.

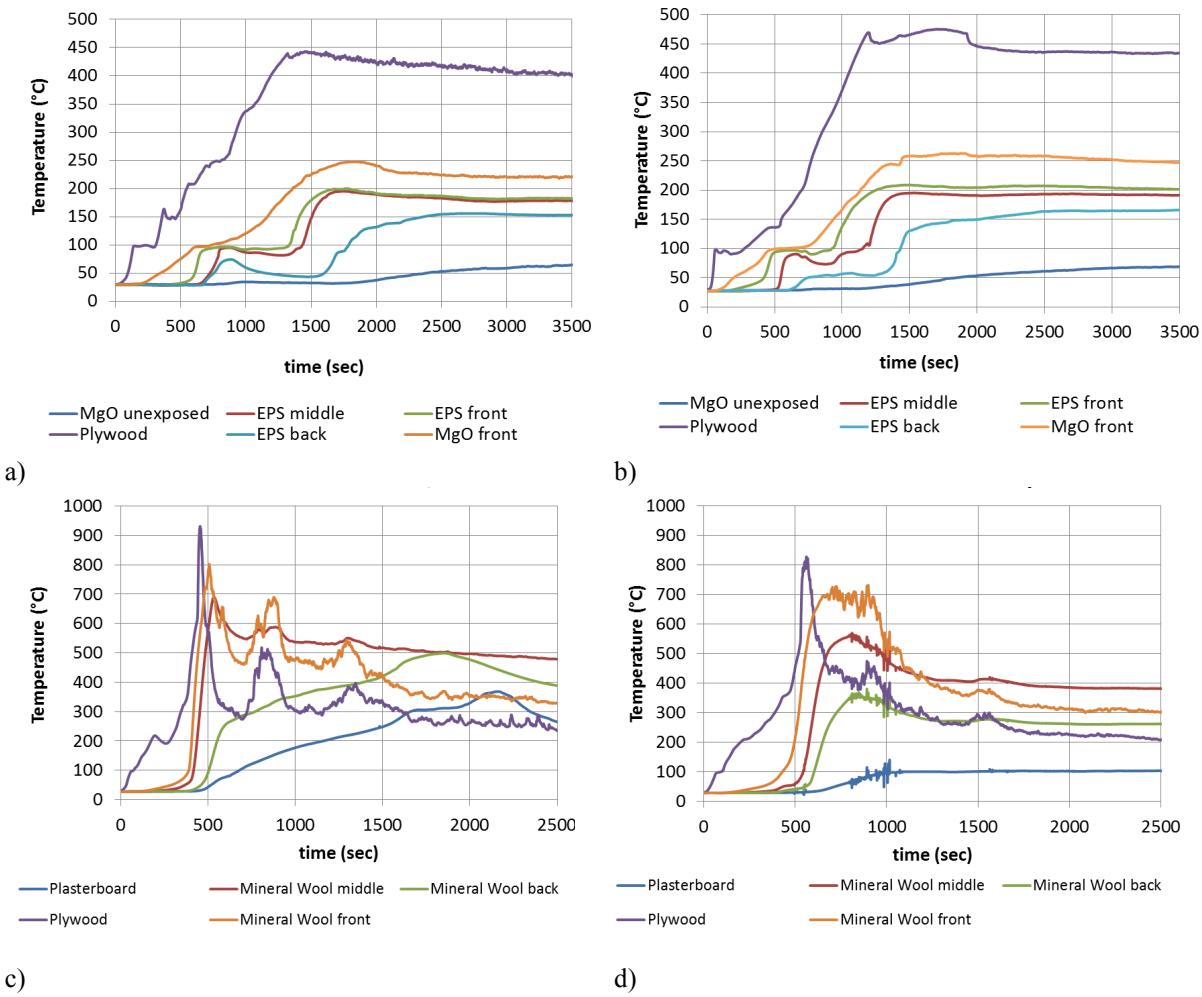

Figure 12 Temperature histories measured for the materials. a) lbSIP+Ply - A1 subject to 24kW/m² b) lbSIP+Ply - B1 subject to 29kW/m² c) LSF - B1 subject to 29kW/m² d) LSF - A1 subject to 24kW/m².

5.5 Discussion

From Table 8 data both the lbSIP+Ply and LSF exposed plywood time to ignition are similar when the heat flux applied is high (i.e. approx. 40 sec. when heat flux applied is 29kW/m^2). This can be explained because in both cases the thermal wave did not cross the plywood panel completely by the time ignition occurs, so the onset of ignition was not influenced by the effect of posterior layers of the systems. Thus, ignition was driven mainly by the thermal inertia of the plywood in isolation, behaving as a semi-infinite solid. The time to ignition calculated using the apparent thermal inertia extracted from thermal efficiency parameters of both systems result in the same value or lower (i.e. LbSIP+Ply: 40 sec. and LSF: 6 sec.). In this sense, the outcome appears to be conservative since the remaining time for real ignition represents the additional time that can also be considered a safety factor.

However, when lower heat flux values are applied (i.e. 24kW/m^2) the thermal wave had enough time to reach the next layer material without reaching the critical temperature to ignition of the plywood. Under these circumstances, only the LSF plywood layer ignited. With this heat flux, the heat wave appears to cross the plywood layer in both systems, but in the LbSIP+Ply system case the heat wave reaches the MgO layer where the heat is dissipated and significantly removed sideways at areas receiving lower heat flux. This effect cannot happen in the LSF system because all materials behind the plywood have lower thermal conductivities, so the heat cannot go beyond the plywood easily. Hence, the heat gets concentrated within the plywood layer accelerating the rate at which the surface temperature increases rapidly reaching the temperature for ignition. Calculated ignition delay times using empirical properties from insulating parameters derived for the thermal efficiency performance approach are much lower than real values (using the real thermal properties) delivering additional time that is valuable as a safety factor for design.

From Figure 12, and regarding the LSF case temperature histories measured, there are no significant differences on readings except those that may appear from construction imperfections that are different between systems sampled. This is seen in the mineral wool layer whose distribution appeared not to be homogeneous internally. Nevertheless, regarding the lbSIP+Ply case when the system is exposed to 29 kW/m^2 and plywood ignites, heat reaches the EPS layer in 4 min time. However, when the lbSIP+Ply is exposed to a lower heat flux (24 kW/m^2), resulting in no ignition of the plywood panel, the heat takes longer to reach the EPS layer. This can be explained because of the dissipating effect of the MgO layer in between that is highlighted at lower heat fluxes. In any case, it is also seen that once the heat reaches the EPS material the heat wave reaches the bottom of the layer in less than 8 min, shrinking at about 100°C and leaving an air gap. This affects the instrument reading by introducing unwanted disturbances in the thermocouple electrical signal ('noise') which is observed in the temperature history data. After that the EPS melted on the thermocouples, the instruments were unable to measure the temperature in the gas phase accurately. This is represented in the figure as a plateau line after about 2300 sec. According to temperature history records, for the case of EPS as the core material in the SIP system, a conservative failure criterion could be based on the softening point (i.e. 80°C – 100°C) where an air cavity is created compromising the structural performance of the system (and the building). Hence unavoidably losing the encapsulating properties and exposing melted EPS.

6 Conclusions

Through this study, the thermal inertia is used to evaluate in a holistic manner both the building envelope component thermal and fire performance to achieve adequate levels of both occupant's comfort and safety, together with building energy-efficiency. Therefore, this study is proposing a step towards the achievement of holistic design solutions where potential detrimental effects of building design disciplines are effectively controlled by integrated assessments — earlier, more accurately, and more effectively.

To obtain more accurate thermal performance predictions, it was justified the use of a thermal transient assessment approach, which is even necessary when daily temperature cyclic variation is representative parameter of the local climate. Under this thermal approach the ability of materials to store heat makes itself apparent and therefore their ability to react to changing temperature conditions. This effect provides construction materials with additional insulating capabilities where the thermal inertia plays a key role which along with the thermal conductivity of materials, the density and the specific heat of construction materials are deemed into analysis.

The thermal inertia is obtained from the cyclic transmittance u-value and surface admittance y-value properties characterised for a building envelope system. These cyclic insulating properties are obtained by using a numerical model that can be enriched by a small-scale thermal test performed on building systems that include structural elements – thermal bridges and construction imperfections. This is a simple, accessible and data-inclusive method, that also allows a comprehensive validation of existing numerical models from measurements not only obtained externally to the building system tested, as current existing testing methods, but also internally. Ultimately, the integrated method ends up using the measured thermal inertia to predict building components reaction-to-fire performance such as the time to ignition of an exposed surface. The methodology was verified experimentally by using two different wall systems and served to highlight that the integrated method delivers conservative prediction of reaction-to-fire performance. Generally, high values of thermal inertia would benefit fire safety and thermal performance in geographical locations where daily temperature variations are the more relevant indicators. Low values of thermal inertia would decrease fire safety but would benefit the thermal performance of buildings located in climates where outdoor and indoor comfort temperatures differ significantly. Thus, thermal inertia controls the balance of both building performance disciplines.

7 Nomenclature

a	Admittance
A	Area
Ai	Area of the interior
Ae	Area of the exterior
f	decrement factor
h_T	Total heat loss coefficient
k	Thermal conductivity
L	Thickness of a building system
q	Heat flow
q_{net}	Net heat flowing through a system
R_{si}	Internal surface resistance
R_{se}	External surface resistance
R_T	Total thermal resistance
x	Depth of a building system
$\bar{x}$	Depth over total thickness
T	Temperature
$\bar{T}$	Temperature over the cyclic temperature amplitude
T_{amb}	Ambient Temperature
T_{cr}	Critical temperature for ignition
T_{ig}	Temperature for ignition
T_p	Pyrolisis Temperature
T_i	Indoor temperature
T_e	Outdoor temperature
t	Time
$\bar{t}$	Time over the cyclic period
u-value	Cyclic transmittance
U-value	Thermal transmittance
y-value	Surface admittance

ρ	Density
c_p	Specific heat
τ_w	Characteristic time for a building system to reach steady state conditions
τ_c	Period of a cyclic temperature variation

Acknowledgements

This study has been developed thanks to the funding provided by the Australian Research Council's Linkage Scheme, together with the contribution of Happy Haus Pty Ltd, Hutchinson Builders Pty Ltd, Vision Developments Australia Pty Ltd and the Fire laboratory facilities at the School of Civil Engineering of The University of Queensland. The authors appreciate the invaluable effort done by the partners involved in the study. Acknowledgement is also given to Queensland Fire and Emergency Service, Fire Engineering Section for their reviews and guidance.

8 References

[1] T. L. Bergman, F. P. Incropera, D. P. DeWitt, and A. S. Lavine, *Fundamentals of heat and mass transfer*. John Wiley & Sons, 2011.

[2] D. Drysdale, *An introduction to fire dynamics*. John Wiley & Sons, 2011.

[3] M. G. Davies, *Building heat transfer*. John Wiley & Sons, 2004.

[4] A. F. Handbook, "American society of heating, refrigerating and air-conditioning engineers," *Inc.: Atlanta, GA, USA,* 2009.

[5] L. Pérez-Lombard, J. Ortiz, and C. Pout, "A review on buildings energy consumption information," *Energy and buildings,* vol. 40, no. 3, pp. 394-398, 2008.

[6] *BS EN ISO 8990:1996 - Thermal insulation –Determination of steady-state thermal transmission properties – Calibrated and guarded hot box*, 1996.

[7] A. Amundarain, "Assessment of the thermal efficiency, structure and fire resistance of lightweight building systems for optimized design," *The University of Edinburgh,* p. 37, 2007.

[8] G. Soret, D. Lázaro, J. Carrascal, D. Alvear, M. Aitchison, and J. Torero, "Thermal characterization of building assemblies by means of transient data assimilation," *Energy and Buildings,* 2017.

[9] S. S. J. Rose, "Validating Numerical Calculations against Guarded Hot Box Measurements," *Nordic Journal of Building Physics* vol. 4, 2004.

[10] B. Anderson, "Conventions for U-valuecalculations," *BRE Scotland* 2006.

[11] X. Jin, X. Zhang, Y. Cao, and G. Wang, "Thermal performance evaluation of the wall using heat flux time lag and decrement factor," *Energy and Buildings,* vol. 47, pp. 369-374, 2012.

[12] V. C. L. John Valiulis, "Building Exterior Wall Assembly Flammability: Have we forgotten what we have learned over the past 40 years?," Fire Safe North America2015, Available: http://www.firesafenorthamerica.org/wp-content/uploads/FSNAWhitePaperNFPA285.pdf.

[13] O. Koenigsberger, T. Ingersoll, A. Mayhew, and S. Szoklay, "Manual of tropical housing and building: Climatic Design Part 1," *Orient Longman, London, UK,* 1974.

[14] P. Miers, "Fire Risks From External Cladding Panels – A Perspective From The UK," http://www.probyn-miers.com/perspective/2016/02/fire-risks-from-external-cladding-panels-perspective-from-the-uk/2016, Accessed on: Nov 2016.

[15] T. Simla and W. J. R. E. Stanek, "Reducing The Impact Of Wind Farms On The Electric Power System By The Use Of Energy Storage," 2019.

[16] J. Wang, R. Bras, G. Sivandran, and R. J. G. R. L. Knox, "A simple method for the estimation of thermal inertia," vol. 37, no. 5, 2010.

[17] J. M. Lora, T. Tokano, J. V. d'Ollone, S. Lebonnois, and R. D. J. I. Lorenz, "A model intercomparison of Titan's climate and low-latitude environment," 2019.

[18] C. Cunningham, I. A. Nesnas, and W. L. J. A. R. Whittaker, "Improving slip prediction on mars using thermal inertia measurements," vol. 43, no. 2, pp. 503-521, 2019.

[19] S. V. Szokolay, *Introduction to Architectural Science : The Basis of Sustainable Design*, Third edition ed. Taylor & Francis Ltd, 2014.

[20] H. Ling *et al.*, "Indicators evaluating thermal inertia performance of envelops with phase change material," vol. 122, pp. 175-184, 2016.

[21] W. Yu, B. Li, H. Jia, M. Zhang, D. J. E. Wang, and Buildings, "Application of multi-objective genetic algorithm to optimize energy efficiency and thermal comfort in building design," vol. 88, pp. 135-143, 2015.

[22] N. Aste, F. Leonforte, M. Manfren, and M. J. A. e. Mazzon, "Thermal inertia and energy efficiency–Parametric simulation assessment on a calibrated case study," vol. 145, pp. 111-123, 2015.

[23] Z. Rahimpour, A. Faccani, D. Azuatalam, A. Chapman, and G. J. E. P. Verbič, "Using thermal inertia of buildings with phase change material for demand response," vol. 121, pp. 102-109, 2017.

[24] N. Milbank and J. Harrington-Lynn, *Thermal response and the admittance procedure*. Building Research Establishment, 1974.

[25] C. E. Uglow, "Predictions of Building Thermal Performance Using The Building Research Establismnet (UK) 'Admittance' based method," 1981.

[26] K. Butcher and B. Craig, *Environmental Design: CIBSE Guide A*. Chartered Institution of Building Services Engineers, 2015.

[27] H. Asan, "Numerical computation of time lags and decrement factors for different building materials," *building and environment,* vol. 41, no. 5, pp. 615-620, 2006.

[28] S.-C. Ng, K.-S. Low, and N.-H. Tioh, "Newspaper sandwiched aerated lightweight concrete wall panels—Thermal inertia, transient thermal behavior and surface temperature prediction," *Energy and Buildings,* vol. 43, no. 7, pp. 1636-1645, 2011.

[29] M. Ibrahim, P. H. Biwole, E. Wurtz, and P. Achard, "Limiting windows offset thermal bridge losses using a new insulating coating," *Applied Energy,* vol. 123, pp. 220-231, 2014.

[30] G. Evola, L. Marletta, S. Natarajan, and E. M. J. E. P. Patanè, "Thermal inertia of heavyweight traditional buildings: Experimental measurements and simulated scenarios," vol. 133, pp. 42-52, 2017.

[31] J. Fernandes, R. Mateus, H. Gervásio, S. M. Silva, and L. J. R. E. Bragança, "Passive strategies used in Southern Portugal vernacular rammed earth buildings and their influence in thermal performance," vol. 142, pp. 345-363, 2019.
[32] G. Soret, J. Tonino, J. Torero, and M. Aitchison, "Towards optimizing thermal performance of prefabricated houses in Australian climates," in *3rd Annual International Conference Architecture and Civil Engineering (ACE 2015)*, 2015, vol. 1, pp. 186-193: Global Science and Technology Forum (GSTF).
[33] E. ISO, "13791: 2004," *Thermal performance of buildings—Calculation of internal temperatures of a room in summer without mechanical cooling—General criteria and validation procedures (ISO,* vol. 13791, 2004.
[34] E. ISO, "13792: Thermal performance of buildings-Calculation of internal temperatures of a room in summer without mechanical cooling-Simplified methods," *European Committee for Standardization. Brussels,* 2005.
[35] E. ISO, "13786: 2007--Thermal performance of building components--Dynamic thermal characteristics--Calculation methods," vol. 27, 2007.
[36] J. Torero, "Flaming ignition of solid fuels," in *SFPE Handbook of Fire Protection Engineering*: Springer, 2016, pp. 633-661.
[37] J. P. Hidalgo, S. Welch, and J. L. Torero, "Performance criteria for the fire safe use of thermal insulation in buildings," *Construction and Building Materials,* vol. 100, pp. 285-297, 2015.
[38] B. Karlsson and J. Quintiere, *Enclosure fire dynamics*. CRC press, 1999.
[39] W. Brown and D. Stephenson, "Guarded hot box procedure for determining the dynamic response of full-scale wall specimens- Part I," in *the 1993 Winter Meeting of ASHRAE Transactions. Part 1*, 1993, pp. 632-642.
[40] K. Martin, A. Campos-Celador, C. Escudero, I. Gómez, and J. Sala, "Analysis of a thermal bridge in a guarded hot box testing facility," *Energy and Buildings,* vol. 50, pp. 139-149, 2012.
[41] W. Brown and D. Stephenson, "Guarded hot box measurements of the dynamic heat transmission characteristics of seven wall specimens-Part II," *ASHRAE Transactions,* vol. 99, no. 1, pp. 643-660, 1993.
[42] J. Sala, A. Urresti, K. Martín, I. Flores, and A. Apaolaza, "Static and dynamic thermal characterisation of a hollow brick wall: Tests and numerical analysis," *Energy and Buildings,* vol. 40, no. 8, pp. 1513-1520, 2008.
[43] F. Kuznik and J. Virgone, "Experimental assessment of a phase change material for wall building use," *Applied Energy,* vol. 86, no. 10, pp. 2038-2046, 2009.
[44] S. Martínez, A. Erkoreka, P. Eguía, E. Granada, and L. Febrero, "Energy characterization of a PASLINK test cell with a gravel covered roof using a novel methodology: Sensitivity analysis and Bayesian calibration," *Journal of Building Engineering,* vol. 22, pp. 1-11, 2019.
[45] E. Hahne and R. Pfluger, "Improvements on PASSYS test cells," *Solar Energy,* vol. 58, no. 4-6, pp. 239-246, 1996.
[46] M. J. Jiménez and H. Bloem, "Energy Performance Assessment of Buildings and Building Components. Guidelines for Data Analysis from Dynamic Experimental Campaigns Part 1: Physical Aspects," *Energy Procedia,* vol. 78, pp. 3306-3311, 2015.
[47] A. Erkoreka, J. Bloem, C. Escudero, K. Martin, and J. Sala, "Optimizing full scale dynamic testing of building components: measurement sensors and monitoring systems," *Energy Procedia,* vol. 78, pp. 1738-1743, 2015.
[48] P. Strachan, "Model validation using the PASSYS test cells," *Building and Environment,* vol. 28, no. 2, pp. 153-165, 1993.
[49] G. Cattarin, F. Causone, A. Kindinis, and L. Pagliano, "Outdoor test cells for building envelope experimental characterisation–A literature review," *Renewable and Sustainable Energy Reviews,* vol. 54, pp. 606-625, 2016.
[50] C. Buratti, E. Belloni, L. Lunghi, and M. Barbanera, "Thermal Conductivity Measurements By Means of a New 'Small Hot-Box'Apparatus: Manufacturing, Calibration and Preliminary Experimental Tests on Different Materials," *International Journal of Thermophysics,* vol. 37, no. 5, pp. 1-23, 2016.
[51] P. Modi, R. Bushehri, C. Georgantopoulou, and L. Mavromatidis, "Design and development of a mini scale hot box for thermal efficiency evaluation of an insulation building block prototype used in Bahrain," *Advances in Building Energy Research,* vol. 11, no. 1, pp. 130-151, 2017.
[52] D. G. Stephenson, "Thermal radiation and its effect on the heating and cooling of Buildings," Report No. 121 of the Building Research 1957.
[53] C. Maluk, L. Bisby, M. Krajcovic, and J. L. Torero, "A heat-transfer rate inducing system (H-TRIS) test method," *Fire Safety Journal,* 2016.
[54] A. Cowlard, A. Bittern, C. Abecassis-Empis, and J. L. Torero, "Some considerations for the fire safe design of tall buildings," *International Journal of High-Rise Buildings,* vol. 2, no. 1, pp. 63-77, 2013.
[55] J. Tonino, "Developing a methodology to investigate the thermal performance of prefabricated housing wall panels using finite element analysis," Bachelor degree, The University of Queensland, 2014.
[56] P. Johansson, B. Adl-Zarrabi, and C.-E. Hagentoft, "Using transient plane source sensor for determination of thermal properties of vacuum insulation panels," *Frontiers of Architectural Research,* vol. 1, no. 4, pp. 334-340, 2012.
[57] G. Mao and G. Johannesson, "Dynamic calculation of thermal bridges," *Energy and Buildings,* vol. 26, no. 3, pp. 233-240, 1997.
[58] E. ASTM, "1321-93,"," *Standard Test Method for Determining Material Ignition and Flame Spread Properties," Annual Book of ASTM Standards,* vol. 4, 1996.
[59] N. Boonmee and J. Quintiere, "Glowing and flaming autoignition of wood," *Proceedings of the Combustion Institute,* vol. 29, no. 1, pp. 289-296, 2002.